Effect of Computation Parameters on BVI Noise Prediction Using HART II Motion Data

Choongmo Yang[*], and Takashi Aoyama[**]

[*]Numerical Analysis Group, Japan Aerospace Exploration Agency, Tokyo, Japan
(Tel : +81-42-240-3309; E-mail: yang@chofu.jaxa.jp)
[**]Numerical Analysis Group, Japan Aerospace Exploration Agency, Tokyo, Japan
(Tel : +81-42-240-3229; E-mail: aoyama@chofu.jaxa.jp)

Abstract

JAXA has been developing its own CFD code to solve full helicopter simulation using accurate flow solver and acoustic solver. The previous researches examined the effect of aero-elastic deformation on the more realistic aerodynamic and acoustic prediction by using HART II motion data, which includes motion information of flapping, lead-lag, and torsion deformations. As for the CFD computation, a moving overlapped grid system is used with three different types of grids (blade grid, inner and outer background grids). Acoustic signal is calculated by an acoustic code based on Ffowcs Williams and Hawkings (FW-H) formulation using the pressure distribution on blade surface obtained by the CFD code as input data. In the present research, several parameters of computation are checked in detail to understand the effects on each parameter on BVI noise when the blade motion is prescribed from the measured data. The effect of these parameters, including grid dependency, fairing effect by fuselage presence, and effect of individual blade motion are discussed. The results show the comparison of unsteady blade loading and BVI noises for baseline case, minimum vibration case, and minimum noise case between calculation and experiment. This research will help the researcher to improve the ability of their own CFD code to predict BVI noise by capturing tip vortex exactly.

Keywords: BVI noise, HART II experiment, CFD, Moving overlapped grid

1. INTRODUCTION

Helicopters are used in various fields such as emergency medical service (EMS), fast and efficient passenger and cargo shuttle, fire fighting, disaster relief, surveillance missions, and so on because of its aviation capabilities in hovering and VTOL. However, noise, cost, and visual flight rules (VFR) problems prevent helicopters from being widely used as a means of inter-city transportation in densely populated area. Many researchers have been and are engaging in the research and development for much wider use of helicopters in the future. FAA is promoting "Rotorcraft Research and Development Initiative 10-year plan[1]" with the objective of developing and demonstrating technologies to enable highly reliable, cost-effective, and environmentally friendly rotorcraft. Also Europe is running "FriendCOPTER Project[2]" as an integrated research project aiming at the development of an environmentally friendly helicopter by focusing on noise and vibration reduction.

To achieve these goals, one of the most important parts in helicopter research is the improved understanding and prediction of its rotor wake aerodynamics. Compared to the fixed wing aircraft, helicopter experiences much more complicated wake from rotor according to the operating states and flight conditions. These complicated wakes have a strong effect on vibration and noise[3] through the changes of air-loads, especially when the wakes remain near rotor-disc during descending flight for landing or maneuver. A great number of different techniques have been used to analyze rotor wake more accurately including analytical, numerical, and experimental approaches, and Ref. 4 shows good reviews on the past and ongoing researches on rotor wakes.

Considering the Blade-Vortex Interaction (BVI) noise, which is known as the most annoying helicopter noises during terminal operations, accurate wake analysis is essential to predict this noise accurately. BVI noise is generated by impulsive pressure fluctuations on main rotor blades when they interact with tip vortices shed by the preceding blades. When the distance between the blade and vortex center, which is called as miss-distance, becomes small at moderate descent angles, strong BVI noise is radiated during conventional approach flight conditions. Many researches including experimental and computational activities have been conducted to achieve a better understanding of BVI noise.

As one of the most efficient analytical tools for BVI noise prediction[5,6], hybrid method combining aerodynamic and acoustic analysis are proposed[7,8]. At first, pressure or the load distribution on rotor blade is calculated by CFD, then subsequent acoustic analysis is executed using the CFD results to predict sound pressure at specified observation points. To simulate accurate BVI, the generation of tip vortex should be accurately simulated considering the complex motion from elastic blade. Then, the trace of tip vortex in three dimensional positions and in time should also be accurately predicted.

To achieve the accurate prediction of tip vortex position in the wake, we can choose one from three typical ways: (1) empirical model used for forward flight such as Beddoes generalized wake model [9], (2) free wake model based on vortex theory [10, 11], or (3) direct calculation using CFD [8,12]. Empirical model is based on the observation of tip vortex behaviors with benefits of low calculation cost, but needs preliminary validation for applying to the unspecified condition. Free wake model is popularly used because of the availability of well-recognized calculation tools like CAMRAD [10] or UMARC [11], but it has the inevitable limit of potential flow assumption. Direct calculation of tip vortex using CFD can solve these problems but involves huge calculation cost. The choice of method depends on the research conditions such as computer resources, computation time, or required precision. The authors have been developing their own CFD code using flow solver and acoustic solver to predict accurate BVI noise. Both approaches using empirical model and direct CFD have been conducted by authors to capture accurate tip vortices. Previous researches have shown its ability to capture the accurate tip vortex traces in several problems [13-16].

Elasticity problems should be considered to predict accurate BVI generated by tip vortex from elastic blades. Lim and etc.[17-18] shows excellent results in CFD/CSD coupling using OVERFLOW-2 and CAMRAD II codes. Our final goal is, of course, to construct an analysis tool by coupling CFD and elasticity. But there exist several stages of error, which is difficult to be separated into each effect on BVI noise output. To achieve accurate prediction, we need to clear the questions of each stage as followings: (1) Can accurate blade motion be simulated by simulation by CFD and elasticity? (2) If the blade motion is correct, can CFD capture the trace of tip vortex accurately? and (3) Can acoustic code predict BVI noise correctly from obtained pressure data? By separating three questions in part, we can concentrate to enhance prediction tool of each stage.

The present paper focuses primarily on the second stage using our CFD code. As the middle step for full coupling aero-elastic analysis, we use elastic blade motion data, which can be captured from specified blade motion by experiment such as HART II project. The objective is to predict BVI noise from the specified elastic blade motion which is measured in experiment to avoid the uncertainty from the aero-elastic analysis.

2. NUMERICAL METHODS

2.1 Overlapped Grid System

A moving overlapped grid system with three different types of grids (rotor grid, inner and outer background grids) is used to simulate BVI of helicopter. Figure 1 shows a perspective view of grid system for the whole computational domain of grid system to solve full helicopter configuration[19]. The body-fitted blade grid in O-H topology moves according to the blade motion such as rotation, flapping, feathering, and lead-lagging. Active flap, which is located at the specified geometric position, oscillates according to the phase, frequency, and amplitude of flap motion. The main-rotor blade grids are generated in each time step of CFD calculation according to the motion of active flap. Concerning the gaps between the main blade and the active flap part, the gaps in span-wise direction are precisely modeled by clustering grid points around the gaps while the gap in chord-wise direction is neglected. The elastic motion of blade is neglected because blades with rigid body are considered here. The flow data are exchanged between the inner background grid and outer background grid, the blade grids, and the fuselage grid. The inner background grid is placed around the rotor disk. The outer background grid covers the whole computation region with a sparse grid density.

Table 1 shows the specification of each grid in the case of 4-bladed rotor with/without fuselage for HART II calculation. The number of blade grid is considerably increased in span-wise direction to match the grid density of the blade grid with that of the inner background grid. Most of the grid points are concentrated in inner-background grid, which captures the trace of tip vortex during several rotations. And three different inner-background grids are used to check the grid dependency. The each grid spacing of coarse, medium, and fine inner background grid corresponds to 0.17c (=0.0105R), 0.099c (=0.006R), and 0.066c (=0.004R), respectively, where c and R are the blade chord length and rotor radius, respectively.

Table 1 Specifications of grid system

Grid type	(X×Y×Z) = number of grid points			
	rotor only			with fuselage
	coarse	medium	fine	medium
Inner background grid	290×230×50 = 3,335,000	450×400×80 = 14,400,000	750×580×140 = 60,900,000	480×400×200 = 38,400,000
Outer background grid	83×79×49 = 321,293			100×80×70 = 560,000
Blade grid	(chord×normal×span) × blade (141×25×131) × 4 = 1,899,500			
Fuselage grid	-	-	-	71×21×83 = 123,753
Total	~5,560,000 points	~16,600,000 points	~61,400,000 points	~41,000,000 points
Inner background spacing	0.17c (=0.0105R)	0.099c (=0.006R)	0.066c (=0.004R)	0.099c (=0.006R)

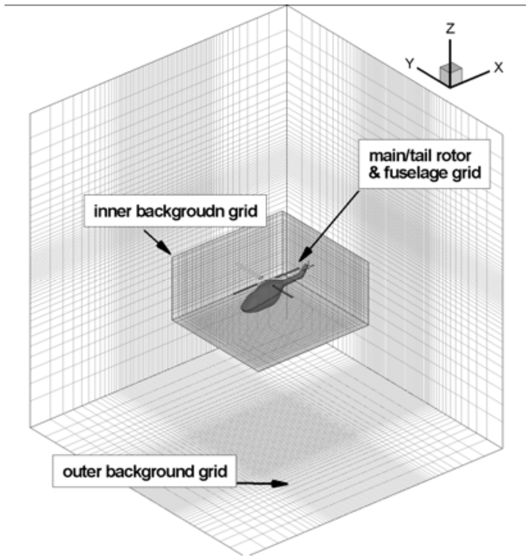

Fig. 1 Perspective view of grid system

2.2 Aerodynamic Solver

A three-dimensional unsteady flow solver for the compressible Euler equation is used to analyze the detailed behavior of tip vortex.

For the calculation of blade grid, the governing equations are discretized in the delta form using Euler backward time differencing. A diagonalized approximate factorization method, which utilizes an upwind flux-split technique, is used for the implicit left-hand-side for spatial differencing. In addition, an upwind scheme based on TVD is applied for the explicit right-hand-side terms. Each operator is decomposed into the product of lower and upper bi-diagonal matrices by using diagonally dominant factorization. For unsteady calculations, the Newton iterative method is used to reduce the residual in each time-step. The number of Newton sub-iterations is four in the present calculations. A detailed derivation of the governing equation and numerical schemes is described in a previous work[20]. The typical resolution in the azimuthal direction is approximately 17000 per revolution, which corresponds to the azimuth angle increment of about 0.021°.

In the calculations of the Cartesian background grids, a 4th-order compact MUSCL TVD scheme[21] is used in space discretization. The Simple High-resolution Upwind Scheme (SHUS) [22] is employed to obtain numerical flux, which is one of the Advection Upstream Splitting Method (AUSM) type approximate Riemann solvers and has small numerical diffusion. The four-stage Runge-Kutta method is used for time integration. The free-stream condition is applied for the outer boundary of outer background grid.

Calculations are performed using Central Numerical Simulation System (CeNSS), which is the main engine of the third-generation numerical simulator of JAXA. It is composed of high performance UNIX servers, FUJITSU PRIMEPOWERs, which are connected by a crossbar network. CeNSS has 9TFLOPS peak performance, 3TB memory, 50TB disk storage, and 600TB tape archive. It takes about 25 hours to calculate one revolution of a rotor Euler calculation for one test condition with medium size inner-background grid using 36 CPUs, and it needs about 5 revolutions to obtain a fully converged solution. When using fine inner-background grid, it takes about 4 times longer than medium one.

2.3 Acoustic Solver

The prediction method of the far field acoustic pressure is based on the combination of CFD technique with an acoustic equation solver. Although direct computation can be used to get the noise solution directly from the flow calculation with CFD based methods, this is available only in the near field in spite of huge computing cost. At present, the best way is the coupling with the integral method for far-field prediction. Acoustic analogy, which is re-arranged into the Ffowcs Williams-Hawkings Equation, is widely used and still under construction for better applications. Retarded time solution to the Ffowcs-Williams and Hawkings equation, neglecting quadruple noise, can be written in the form of Formulation1 by Farassat[23]. The prediction of rotor noise is conducted in the following procedures: 1) calculation of sound pressure of the noise source, 2) acoustic prediction computation at the observer position, and 3) post-processing of the noise data in the way of sound level using visualization or audible converting.

Hypothesis of the Ffowcs-Williams and Hawkings equation[24] to be satisfied are known that the noise source must lay in low speed flow, and the observer should be located outside of the source region (i.e. outside of the boundary layer, separation flow or wake) in order to avoid the nonlinear effect. In most calculations to compare the results with wind tunnel experiment, the observer moves in the same direction and at the same speed as the noise source. The pressure distribution on the blade surface calculated by the CFD code is stored every 0.5 degrees in azimuth-wise direction as the input data in noise calculation.

3. HART II MOTION DATA

3.1 HART II Project

As a part of international cooperative project of HART II (Higher Harmonic Control Aeroacoustic Rotor Test) [25-27] by German DLR, French ONERA, NASA Langley, and the US Army Aero Flight Dynamics Directorate (AFDD), a comprehensive wind tunnel experiment was conducted in October 2001 with a 40%-geometrically and aeroelastically scaled model of a BO-105 main rotor in the open-jet anechoic test section of the German-Dutch Windtunnel (DNW).

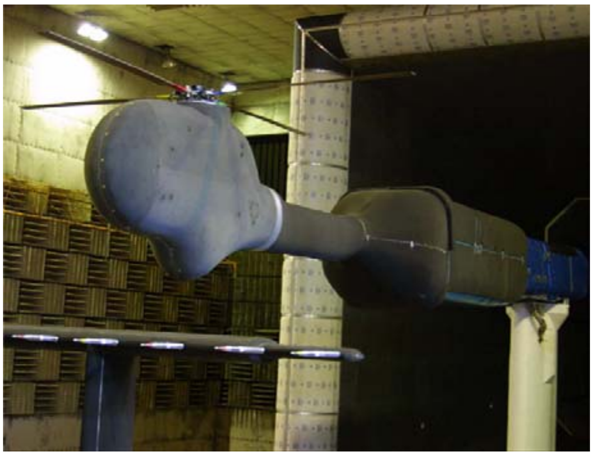

Fig. 2 Arrangement of HART II model in the test section.

The main objective of the program is to investigate the characteristics of rotor wake and its influence on rotor blade-vortex interaction (BVI) noise on the condition with/ without higher harmonic pitch control (HHC). Comprehensive data measurement was carried out to obtain acoustic, rotor wakes, aerodynamic, and blade deformation data with pressure-instrumented blades. Blade position and deflection were also measured using the Stereo Pattern Recognition (SPR) technique[28], which is based on a 3-dimensional reconstruction of visible marker locations by using stereo camera images. An evaluation of these images leads to the spatial position of markers which were attached to each of the four blades and to the bottom of the fuselage. From these measurement, the blade motion parameters in flap, lead-lag and torsion can be evaluated[29]. Figure 2 shows the arrangement of HART II model in the test section including 4 blades and fuselage. A lot of research works on HART II project were reported [28,29], and HART II blade motion data have been used for the research validation on wake capturing, aero-elastics, and aero-acoustics.

3.2 HART II Motion Data Treatment

Three representative cases from HART II experimental data are simulated including baseline (BL) case, minimum noise (MN) case, and minimum vibration (MV) case. In BL case, the blade is operated only with the first order cyclic pitch control, which is the basic condition to be used as a standard to other conditions. In MN and MV cases, higher harmonic cyclic pitch control (HHC) is applied to achieve each objectives: noise reduction for MN case, and vibration reduction for MV case. Test conditions such as blade geometry, flow condition, and blade motion parameters for each case are shown in Table 2.

The HART II motion data includes information of “flapping” (bending perpendicularly with respect to the blade surface), “lead-lag” (forward or backward bending along the blade surface), and “torsion” (twisting around the quarter chord of blade) deformations. These data are available at interval both in space (at eighteen spanwise positions) and in time (at every fifteen degrees of azimuth angle), and thus need to be interpolated for CFD calculation which requires continuous value of blade position both in time and in space. 6th-order Fourier approximation is applied to HART II motion data to get time-continuous data, and third-order spline interpolation is applied to get spanwise continuous data. As an example, Fig. 3 shows measured data and their Fourier approximations of blade deformation at 0.996R spanwise positon for BL case. Figure 3(a) shows the measured and calculated blade motion data including displacement by flapping/lead-lag and rotation by torsion. Figure 3(b) shows the actual vertical/lead-lag position and pitching angle of blade, which is obtained by modifying the upper figure with pre-coning angle and trim condition. The blade motion for one revolution is reconstructed in Fig. 4, where the motion of single blade is drawn at interval of 72 degrees and the deformation of blade is magnified to 5 times of its real value for easy recognition. The calculation grid is generated automatically at each time step according to the deformation of blade.

Table 2 Calculation conditions for BL, MN, and MV cases

Rotor radius, R (m)		2.0	
Blade chord length, c (m)		0.121	
Twist angle ($/R$)		-8.0°	
Precone angle, β_0		2.5°	
Thrust Coefficient, C_T		0.0044	
Tip Mach number, M_{tip}		0.6387	
Inflow ratio, μ		0.15	
Angle of tip path plane, α_{TPP}		4.5°	
Blade motion data	**BL**	**MN**	**MV**
Collective pitch angle, θ_0	3.2°	3.15°	3.16°
Lateral cyclic pitch angle, θ_{1C}	2.0°	2.04°	2.04°
Longitudinal cyclic pitch angle, θ_{1S}	-1.1°	-1.07°	-1.11°
HHC lateral cyclic pitch angle, θ_{3C}	0°	0.41°	-0.79°
HHC long. cyclic pitch angle, θ_{3S}	0°	-0.70°	0°

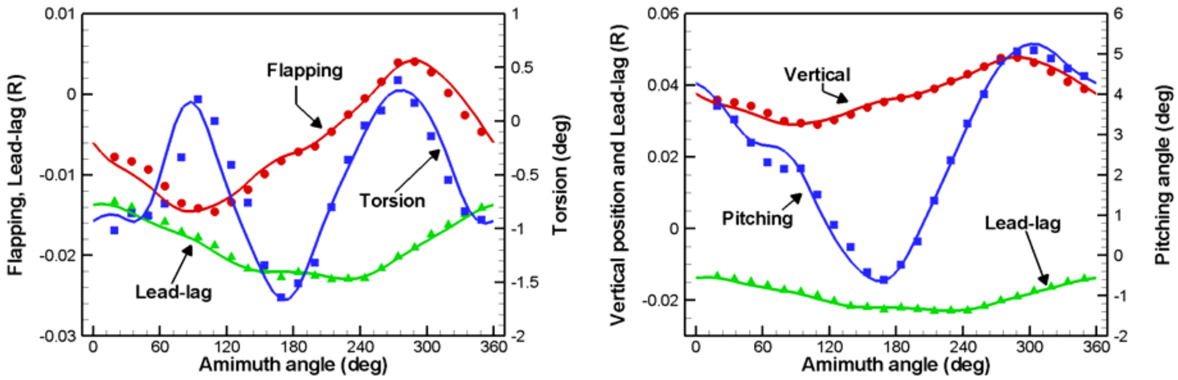

(a) (b)

Fig. 3 Measured values (symbols) and their Fourier approximations (lines) of blade deformation at 0.996R spanwise positon for BL case.

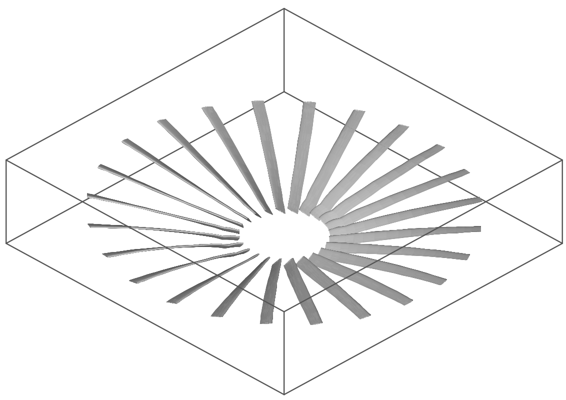

Fig. 4 Reconstructed blade motion referring to HART II motion data for BL case.

4. RESULTS AND DISCUSSION

4.1 Effect of Elastic Motion (BL case)

To see the effect of elastic blade motion, three test conditions are used and compared with HART II experiment results. The original tip path plane angle of HART II experiment is 5.3 degrees, but it is modified to 4.5 degrees[27] to adjust so called “fairing effect”. It comes from hub/fuselage blockage effects that actually cause the change of induced inflow near the center of the rotor disk. Rigid blade without elastic deformation is used for these two different tip path plane angles as fro reference. Then an elastic blade motion is simulated using specified blade motion data from HART II measurement. Figure 5 shows the comparison of blade loading coefficient (C_nM^2) which is defined as

$$C_n M^2 = \frac{2}{\rho a_\infty^2 c}\left(\sum_{low} P_{low}\Delta x_{low} - \sum_{up} P_{up}\Delta x_{up}\right)$$

at 87% spanwise position with/without elastic deformation for BL case. All three cases show fluctuations by BVI in both advancing side (around azimuthal angle of 50 degrees) and retreating side (around azimuthal angle of 300 degrees). The main difference from the elastic deformation is shown around front area of rotor disc, i.e. from 120 to 240 degrees of azimuthal angle. The blade loading with blade elastic deformation drops quite amount compared to the two results with rigid blade, which shows the same tendency with the torsion of elastic blade as shown in Fig.3(a). As a result, calculated coefficient of blade loading with elastic motion shows better agreement with measured one.

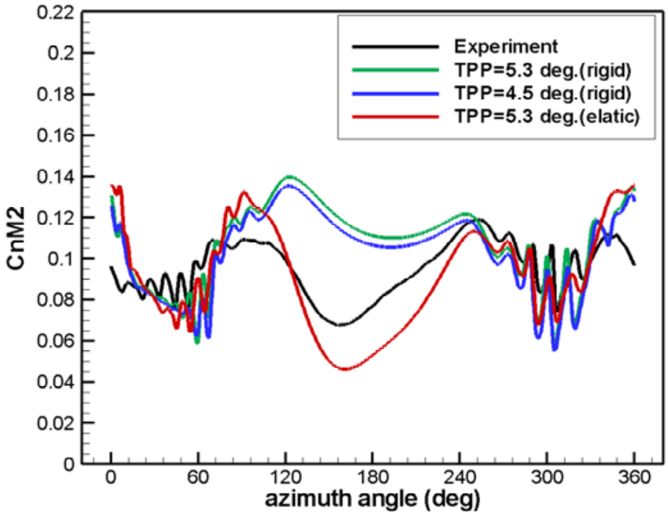

Fig. 5 Measured and calculated coefficient of blade loading at 87% spanwise position with/without elastic deformation for BL case.

4.2 Effect of Grid Dependency (BL case)

One of the important and difficult things for accurate tip vortex capturing is to maintain the strength of tip vortex for several revolutions within computational domain without numerical dissipation. For present method, tip vortex is generated in blade grid, and then transferred to background grid so that it should remain less dissipated during computation. To check grid dependency, three different inner-background grids are used as already shown in Table 1. Figure 6 shows the comparison of C_nM^2 at 87% spanwise position for BL case according to the different inner background grid. All calculated results show similar pattern in general, but zoomed views near BVI positions show the effect of grid dependency more clearly. As grid gets finer, the gradient of pressure gets steeper when BVI occurs in advancing side and retreating side, which is directly related to the strong BVI noise. The results of fine grid shows better agreement in peak positions and the detailed behavior of tip vortex, but the peak-to-peak magnitude of BVI fluctuations seems over-estimated, which is related to the over-estimation of sound pressure in the end. It may be explained by the inviscid assumption of present Euler calculation. Figure 7 compares the gradient of blade loading coefficient at 87% spanwise position for BL case with different grid for measured and calculated results.

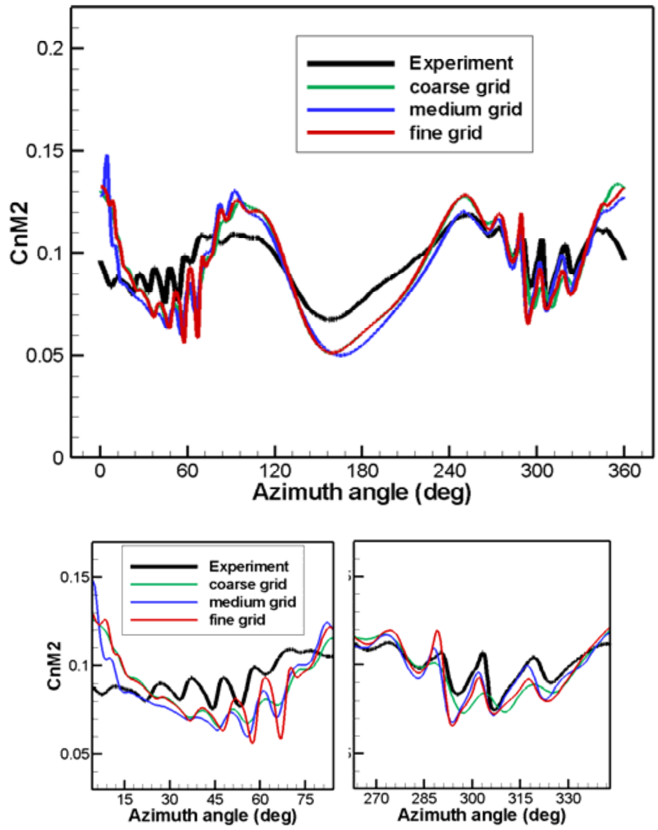

Fig. 6 Comparison of grid dependency for measured and calculated coefficient of blade loading at 87% spanwise position for BL case.

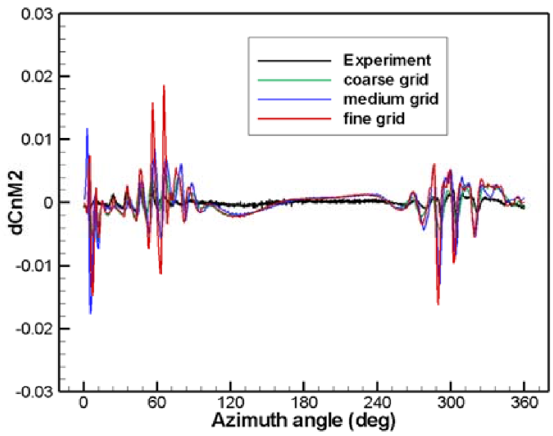

Fig. 7 Comparison of grid dependency for measured and calculated coefficient gradient of blade loading at 87% spanwise position for BL case.

4.3 Fairing Effect (BL case)

As mentioned before, one of the ways to consider faring effect is to modify the tip path plane angle. But the fairing effect doesn't affect whole rotor disc with same magnitude, rather partially affects according to hub/fuselage existence. So the better way is to include the fuselage itself into computation, which increases computation cost a lot because the large fuselage needs more computational domain, i.e., more grid points compared to that of flat blade. At the present research, the effect of fuselage is simulated using HART II fuselage model[26] in computation. The tip path plane angle is restored to the original one of HART II experiment. Figure 8 shows the comparison of CnM2 at at 87% spanwise position for BL case with/without fuselage for medium size of inner background grid. Overall pattern shows similar in general, but the three improvements are achieved using fuselage model. At first, front area of rotor disk around 180 degrees of azimuthal angle shows better agreement with measured one. At second, unrealistic peak around 0 degree of azimuthal angle, which was shown in previous results, disappears. Finally, the pressure oscillations of BVIs in both advancing side and retreating side show better agreements with measured data.

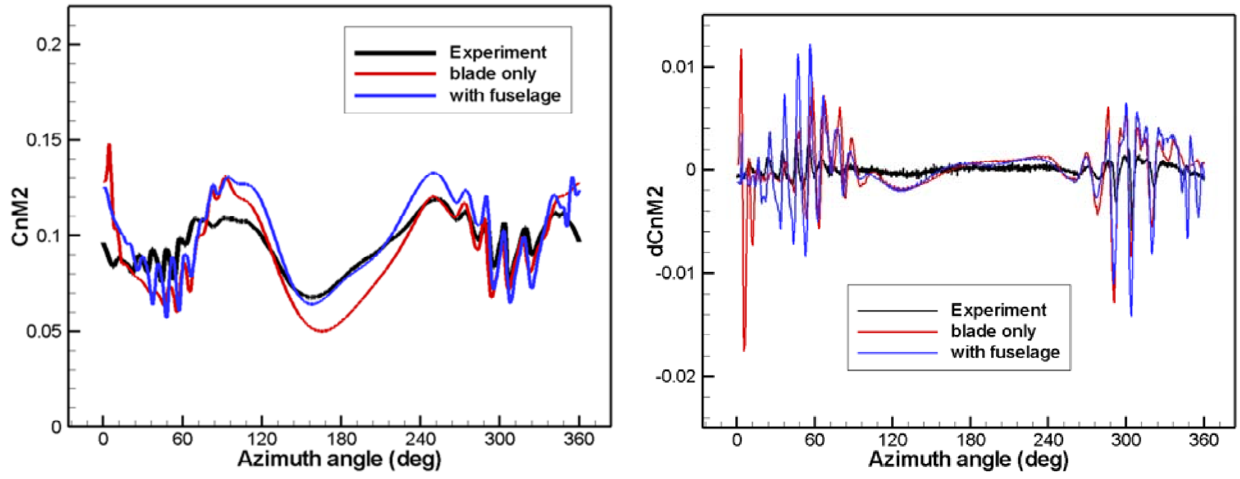

(a) $C_n M^2$ (b) $\frac{d}{d\psi}\left(C_n M^2\right)$

Fig. 8 Measured and calculated coefficient and its gradient of blade loading at 87% spanwise position for BL case.

4.4 Different blade motion for 4 blades

In the HART II experiment, unsteady pressure were measured on two blades, the reference blade (No.1), and the blade preceeding it (No. 4). Owing to these pressure sensors, the motions of 4 blades according to the blade number are slightly different. However, most of the HART II computation uses the reference blade data only. In this section, the effect of 4 different blade motions altogether is checked. Figure 9(a) shows the comparison of CnM2 at at 87% spanwise position for BL case with/without 4 blade motions for medium size of inner background grid. Calculated pressure on the first blade among 4 different blade motions is very similar to the pressure of reference blade with unified blade motion. The pressure on 4th blade shows quite a discrepancy from that of first blade, but still much closer than other two blades. When the effect of fuselage is also included, the calculated blade loadings show better prediction as shown in Fig. 9(b). Overall pattern shows similar in general, but low frequency blade loading from 130 to 240 degrees shows much progress. Also, high frequency blade loadings from BVI in both advancing side and retreating side approach to the experiment.

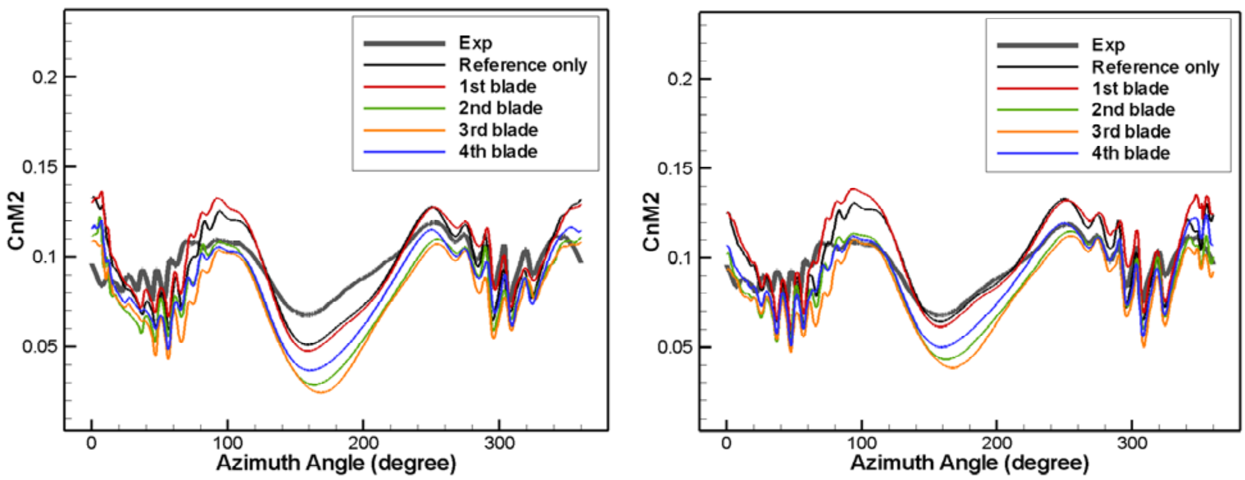

(a) without fuselage (b) with fuselage

Fig. 9 Effect of 4 different blade motions on blade loading at 87% spanwise position for BL case.

4.5 Sound Pressure Calculation

Using the pressure loading on blade surface, sound pressure is calculated using acoustic solver. Figure 10 shows the calculated sound pressure before/after high pass filter for BL case with medium grid. After 4/rev high pass filtering, average sound pressure is adjusted to zero, and low frequency blade loading is effectively removed to distinguish the high frequency peaks including BVI peaks.

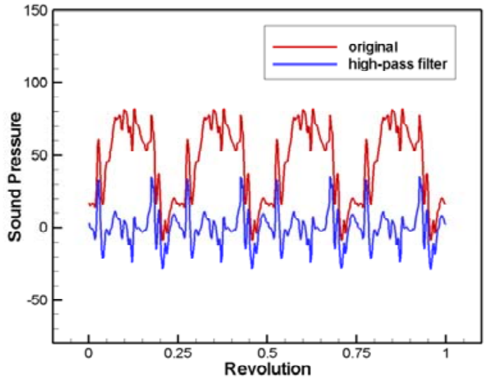

Fig. 10 Calculated sound pressure before/after high pass filter at 4/rev for BL case with medium grid.

Figure 11 shows the comparison of differential pressure (ΔP=P_{up}-P_{low}) distribution on blade leading edge. The lower surface pressure and upper surface pressure are given at 3% chordwise position of blade and ΔP is plotted both spanwisely and azimuthwisely for one revolution. Figure 11(a) shows the measured one from HART II project experiment for BL case. Figure 11(b)-(d) shows the results with several calculations of elastic deformation with different grid, and Fig.11 (e) for the case with fuselage. Characteristic stripe patterns are observed in all figures, especially in the early stage of advancing side and in the late stage of retreating side. The positions of stripes in these regions are similar between calculation and experiment, indicating BVI is occurring in the same phase between them. It is consistent with the result of blade loading in Figs. 5-7. Compared to the result of coarse grid, those of medium grid or fine grid show strong stripes, i.e. strong BVIs, and the result with fuselage shows the best agreement with the measured one. For all cases, effect of root tip vortex appears around azimuthal angle of 0 degree compared to the experiment which includes hub in root region suppressing excessive tip vortex from blade root tip., This effect of root tip vortex cannot be totally dismissed for the case with fuselage because the hub is still not considers, even the blade loading shows much improvement.

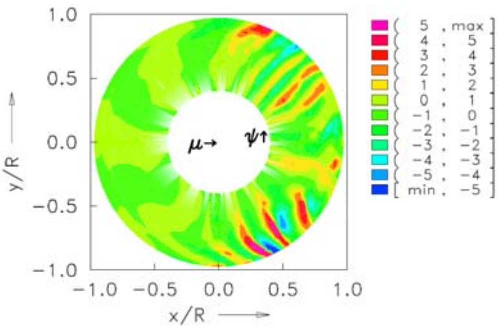

(a) HART Experiment

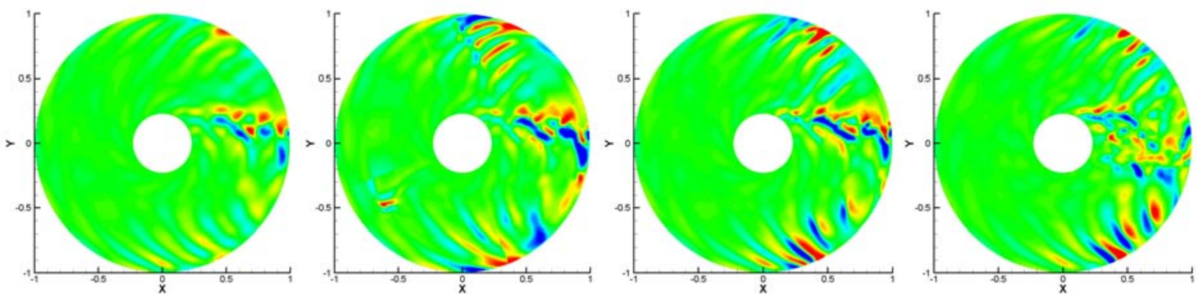

(b) coarse grid (c) medium grid (d) fine grid (e) with fuselage

Fig. 11 Comparison of leading edge differential pressure distribution for BL case.

The unsteady blade loading on blade surface is propagated to farfield as noise, and especially the gradient of surface pressure is directly related to the BVI noise. Figure 12 compares the measured and calculated blade loading coeffici ent and its gradient at 87% spanwise position for various parametric cases in BL case. As the grid become finer, the BVI becomes stronger. The Overall computation results show over-predicted values than experiment, which means that the BVI of computation is stronger that the experimental results. The reason is thought to be the assumption of inviscid flow. Figure 13 comparison of measure and calculated sound pressure for BL case using high pass filter at 4/rev according to different conditions. The peak level of sound pressure is quite dependent on the inner-background grid size, and the results show that the proper grid size, at least medium grid, should be used to predict BVI sound pressure. The result of fine inner- background grid shows over-estimated sound pressure in positive peak magnitude, which comes from inviscid assumption of Euler calculation, as explained in the previous section. The effect of fuselage is shown as the comparable sound pressure peak to that of fine grid, even the medium inner-background grid is used for the fuselage calculation.

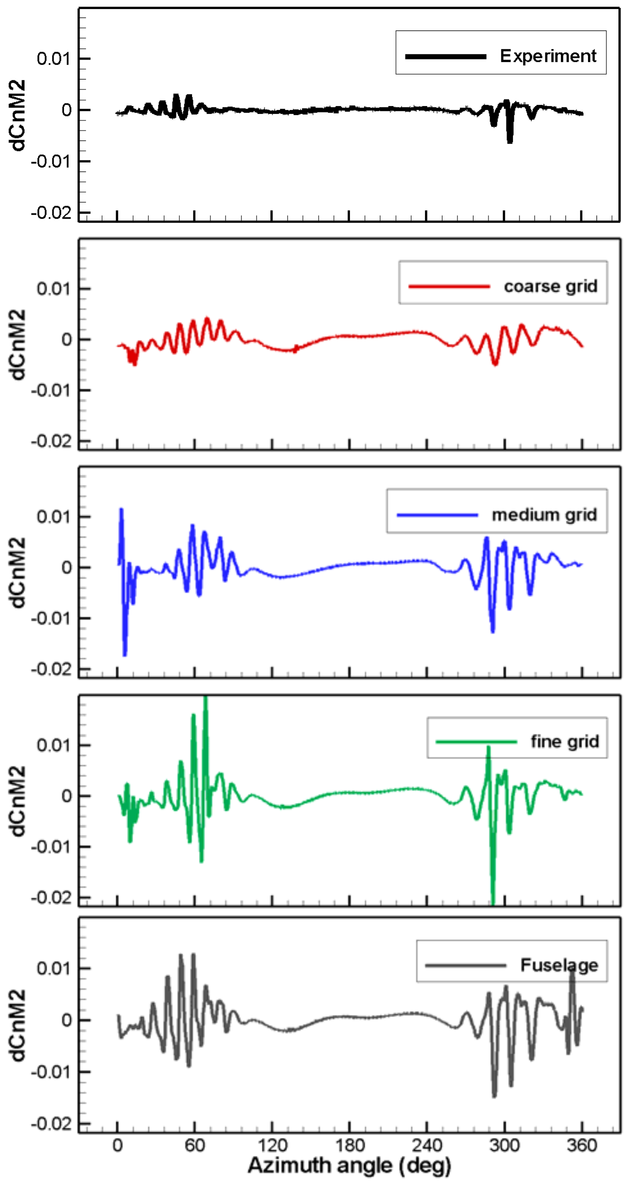

Fig. 12 Measured and calculated $C_n M^2$ and $\frac{d}{d\psi}\left(C_n M^2\right)$ at 87% spanwise position for several parameters of BL case

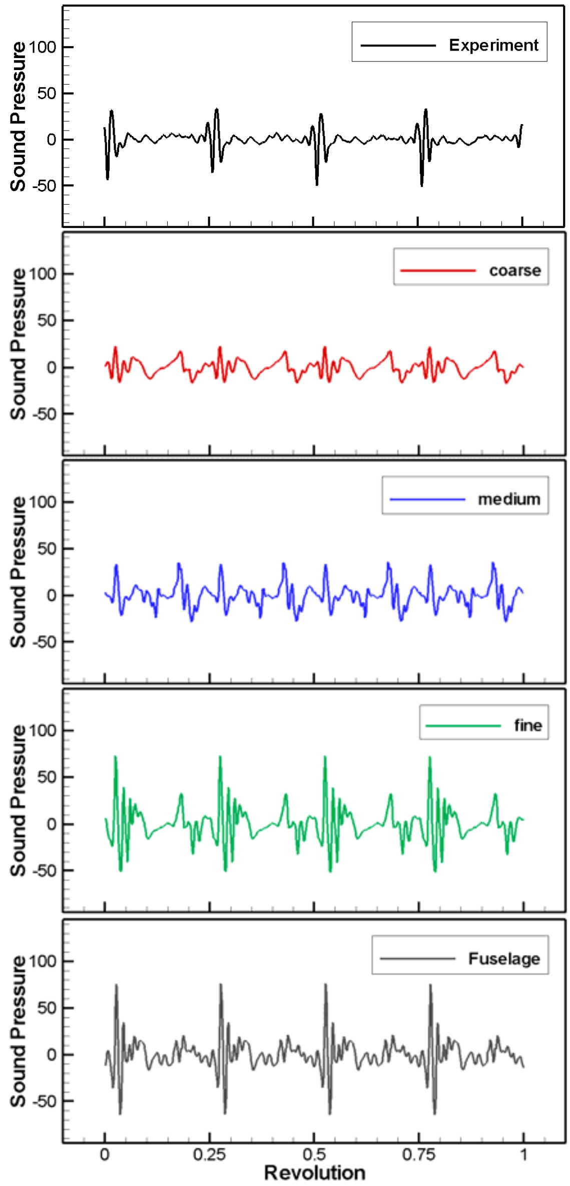

Fig. 13 Measure and calculated sound pressure for BL case using high pass filter at 4/rev.

4.5 MN/MV Cases

Besides base line case, HART II project serves blade motion data for two more cases, minimum noise (MN) case and minimum vibration (MV) case. To check the ability of present analysis method, these two cases are also simulated and compared with experimental data. Figures 13 and 14 compare the results of MV case with experimental result. General pattern and detailed fluctuations from higher harmonic cyclic pitch control fit well to measured data in both advancing side and retreating side. Especially the number and position of loading fluctuations from BVI show remarkable agreement with the measured one. The discrepancy around 180 degrees of azimuthal angle is expected to be improved by including fuselage model from the results of previous section.

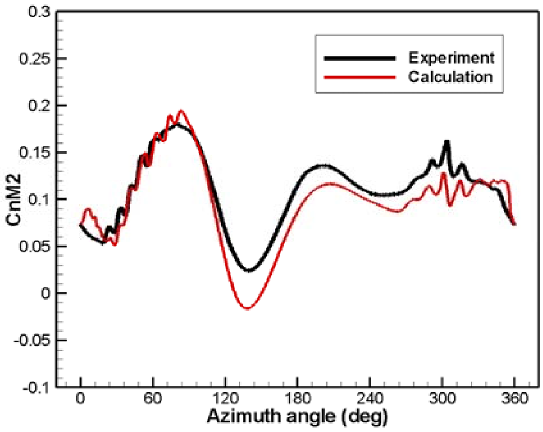

Fig. 13. Measured and calculated coefficient of blade loading at 87% spanwise position for MV case.

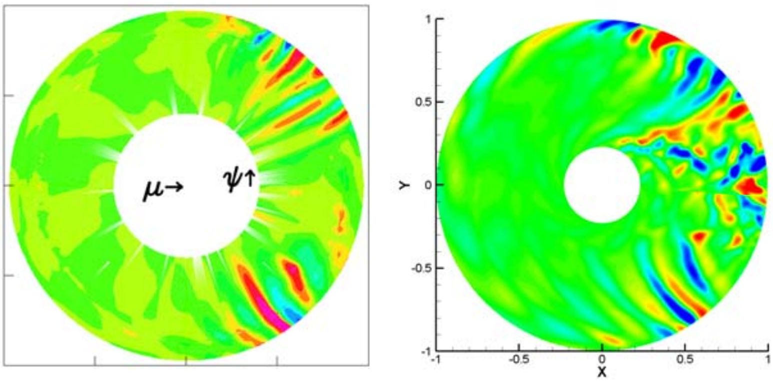

(a) Experiment (b) Calculation

Fig. 14. Comparison of leading edge differential pressure distribution for MV case.

Figures 15 and 16 compare the results of MN case with experimental result. Even detailed fluctuations in Fig. 13 show some discrepancy especially in advancing side compared to measured data, general pattern shows good agreement in terms of the same fluctuation numbers during BVI. From the results of BL case with fuselage, we can predict that leading edge differential pressure distribution in Figs 15 and 16 would show better agreement if the fuselage be included into computation.

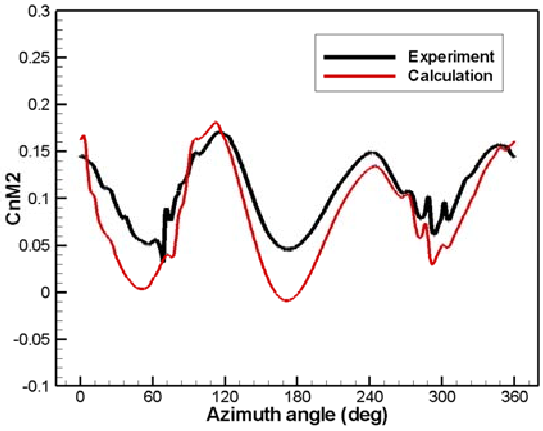

Fig. 15 Measured and calculated coefficient of blade loading at 87% spanwise position for MN case.

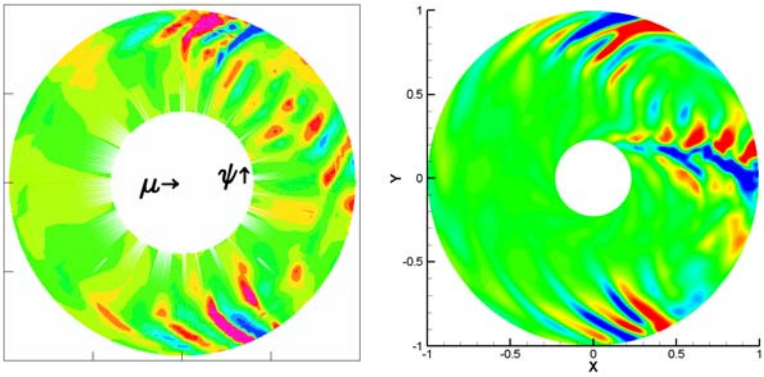

(a) Experiment (b) Calculation

Fig. 16 Comparison of leading edge differential pressure distribution for MN case.

5. CONCLUSIONS

The CFD simulation with elastic blade deformation is conducted using HART II motion data as the middle step for full coupling method of aero-elastic analysis, and the followings can be concluded.

(1) Using the blade elastic deformation data from HART II experiment, the precision of calculation is remarkably enhanced to show good agreement in blade loading and sound pressure of BVI between calculated and measured data. It indicates the ability of present CFD code to capture the trace of tip vortex.
(2) The prediction of BVI blade loading and sound pressure is strongly dependent on the inner-background grid size, and the proper grid size should be used to predict steep pressure gradient from BVI.
(3) By including fuselage grid into computation, fairing effect can be effectively considered to show much enhanced agreement of blade loading and sound pressure with experiment.
(4) The different blade loading for 4 blades according to the pressure sensor installment produces slight change in blade loading compared to the unified blade motion.
(5) The availability of present CFD code is successfully extended using MN/ MV cases to show good agreement with experimental data.

ACKNOWLEDGMENTS

The authors express special thanks to HART II project team for giving us the chance of using their database, and also express special thanks to Dr. van der Wall at DLR Institute of Flight Research, Germany, for his useful advices on the HART II blade motion data.

REFERENCES

[1] http://www.theorator.com/bills108/s309.html

[2] http://www.eurocopter.com/jrotor/69/friendcopter.html

[3] F. Caradonna, et al., "A review of methods for the prediction of BVI noise," *AHS technical specialist' meeting for rotorcraft acoustics and aerodynamics*, 1997.

[4] J. G. Leishman (ed.), "Special Issue on Rotor Wakes," *Journal of Aircraft*, Vol. 39, No.5, 2002.

[5] F. H. Schmitz, Y. H. Yu, "Helicopter impulsive noise: theoretical and experimental status," *Journal of Sound and Vibration* 109(3) pp. 361-422, 1986.

[6] F. Caradonna, C. Kitaplioglu, M. McCluer, J. Baeder, G. Leishman, C. Berezin, J. Visintainer, J. Bridgeman, C. Burley, R. Epstein, A. Lyrintzis, E. Koustavdis, G. Rahier, Y. Delrieux, J. Rule, D. Bliss, "A review of methods for the prediction of BVI noise," *AHS technical specialists' meeting for rotorcraft acoustics and aerodynamics* pp.1-53, 1997.

[7] K.S. Brentner, L. V. Lopes, H. Chen, J. F. Horn, "Near Real-Time Simulation of Rotorcraft Acoustics and Flight Dynamics," *AHS 59th Annual Forum Proceedings*, Phoenix, Arizona, May 6-8, 2003.

[8] A. Ochi, T. Aoyama, S. Saito, E. Shima, E. Yamakawa, "BVI Noise Predictions by Moving Overlapped Grid Method," *AHS 55th Annual Forum Proceedings*, May, 1999.

[9] T. S. Beddoes, "A Wake Model for High Resolution Airloads," *2nd International Conference on Basic Rotorcraft Research*, Triangle Park, NC, 1985.

[10] W. Johnson, "Comprehensive Analytical Model of Rotorcraft Aerodynamics and Dynamics," *Johnson Aeronautics*, Vol. I-VII, Sep, 1998.

[11] http://www.enae.umd.edu/umarc/

[12] R. C. Strawn, E. P. N. Duque, J. Ahmad, "Rotorcraft Aeroacoustics Computations with Overset-Grid CFD Methods," *Journal of American Helicopter Society*, Vol.44, pp.132-140, 1999.

[13] C. Yang, T. Aoyama, and S. Saito, "Numerical Study on BVI Noise Reduction Using Active Flap Control," *31st European Rotorcraft Forum*, No. 24, Florence, Italy, September 2005.

[14] T. Aoyama, C. Yang, and S. Saito, "Numerical Analysis of Active Flap for Noise Reduction Using Moving Overlapped Grid Method", *Journal of American Helicopter Society*, Vol.52, No.3, pp.189-200, 2007.

[15] T. Aoyama, C. Yang, N. Kondo, and S. Saito, "Fundamental CFD Analysis on Main-Rotor/Tail-Rotor Interaction Noise of Helicopters," *Theoretical and Applied Mechanics Japan*, Vol.53, pp.215-220, October 2004.

[16] C. Yang, T. Aoyama, and S. Saito, "Numerical Analysis of Blade-Vortex Interaction Noise in Maneuvering Flight Using Moving Overlapped Grid Method", *62nd Annual Forum of the American Helicopter Society*, Phoenix, AR, May, 2006

[17] J. Lim, T. A. Nygaard, R. Strawn, and M. Potsdam, "Blade-Vortex Interaction Airloads Prediction Using Coupled Computational Fluid and Structural Dynamics," Journal of the American Helicopter Society, Vol. 52, (4), October 2007, pp. 318-328.

[18] J. Lim, "An Assessment of Rotor Dynamics Correlation for Descending Flight Using CFD/CSD Coupled Analysis", *64th Annual Forum of the American Helicopter Society*, Montreal, Canada, May, 2008

[19] C. Yang, T. Aoyama, and S. Saito, "Numerical Analysis of Interaction Noise between Main Rotor and Tail Rotor of Helicopter," *24th Congress of International Council of Aeronautical Science (ICAS)*, Yokohama, Japan, August, 2004

[20] T. Aoyama, K. Kawachi, and S. Saito, "Unsteady Calculation for Flow-field of Helicopter Rotor with Various Tip Shapes," *18th European Rotorcraft Forum*, Paper No. B03, Avignon, France, September 15-18, 1992.

[21] S. Yamamoto, and H. Daiguji, "Higher-Order-Accurate Upwind Schemes for Solving the Compressible Euler and Navier-Stokes Equations," *Journal of Computers & Fluids*, Vol. 22, pp.259-270, 1993.

[22] E. Shima, and T. Jounouchi, "Role of CFD in Aeronautical Engineering (No.14) - AUSM type Upwind Schemes -," NAL SP-34, pp. 7-12, 1999.

[23] Y. Nakamura, and A. Azuma, "Rotational Noise of Helicopter Rotors," *Vertica*, Vol. 3, (3/4), pp.293-316, 1979.

[24] F. Farassat, "Theory of noise generation from moving bodies with an application to helicopter rotors," NASA TR R 451, 1975.

[25] Y. H. Yu, C. Tung, B. van der Wall, H. Pausder, C. Burley, T. Brooks, P. Beaumier, Y. Delrieux, E. Mercker, and K. Pengel, "The HART II Test: Rotor Wakes and Aeroacoustics with Higher-Harmonic Pitch Control (HHC) Inputs – The Joint German/French/Dutch/US Project,|" *58th Annual Forum of the American helicopter Society*, Montreal, Canada, June 11-13, 2002.

[26] B. van der Wall, "2nd HHC Aeroacoustic Rotor Test (HART II)- Part I: Test Documentation -," DLR 1B 111-2003/21, Braunschweig, Germany, 2003

[27] B. van der Wall, and C. Burley, "2nd HHC Aeroacoustic Rotor Test (HART II)- Part II: Representative Results -," DLR 1B 111-2005/3, Braunschweig, Germany, 2005.

[28] O. Schneider, B. van der Wall, and K. Pengel, "HART II Blade Motion Measured by Stereo Pattern Recognition (SPR)," *59th Annual Forum of the American Helicopter Society*, Phoenix, Arizona, May 6-8, 2003.
[29] J. Lim, C. Tung, Y. Yu, C. Burley, T. Brooks, D. Boyd, B. van der Wall, O. Schneider, H. Richard, M. Raffel, P. Beaumier, J. Bailly, Y. Delrieux, K. Pengel, and E. Mercker, "HART II: Prediction of Blade-Vortex Interaction Loading," *29th European Rotorcraft Forum*, Friedrichshafen, Germany, 16-18 September 2003.